The slanted-edge method application in testing the optical resolution of a vision system

G. BOSTAN[a,c], P. E. STERIAN[a,b], T. NECSOIU[c], A. P. BOBEI[a], C. D. SARAFOLEANU[a,d]
[a]*University "Politehnica" of Bucharest, Academic Center for Optical Engineering and Photonics, Faculty of Applied Sciences, Physics Department, Romania.*
[b]*Academy of Romanian Scientists, Bucharest, Romania.*
[c]*OPTOELECTRONICA-2001 SA, Bucharest, Romania*
[d]*"Sfanta Maria" Clinical Hospital, ENT-HNS Department, 37-39, Ion Mihalache Bvd., District 1, Bucharest, Romania*

The article studies the application of the slanted-edge method to test the optical resolution of a system of lens integrated into a robotic vision system and generally for studying a featured optoelectronic device with adaptive optics. The variety of camera usage conditions, including vibrations, degradation of lens coatings, etc. requires resolution verification operations, often on the go or on the fly. The slanted-edge method focuses on soft procedures, allowing for remote resolution control. The described method is useful because of the fact that the camera to be tested does not need necessarily to be dismounted and placed on the test stand. It does not require the use of a special test chart for verifying the resolution. It can also be applied on infrared viewing cameras, thermal imaging camera, X-rays imager, medical imaging and radiological anatomy and in many other control and security applications.

(Received October 1, 2018; accepted February 12, 2019)

Keywords: Slanted-edge method, Spread function, Modulation transfer function, Space frequency response, Optical resolution

1. Introduction

The calculation method of the modulation transfer function for an imaging system has been developed simultaneusly with the progress of new optical sensors for cameras. The use of the slanted-edge method for testing camera resolution has been of interest for researchers before the appearance of digital optical sensors, when photography was done on photographic film [1, 2, 18-23] and the recording of the light gradient from a testing slant edge was performed using the microdensitometer. Currently, the performance of digital optical sensors allows a good enough sampling rate of the light gradient from a slant edge.

2. Basic optical model

2.1. The effect of the diffraction phenomenon on a circular aperture

An area of interest in imaging is the clarity of the images recorded by the optical system, having as main elements the lens system and the optical sensor. When examining a digital camera, we make subjective appreciations on how acceptable the image is. As against the cameras used in robotic vision and various areas of security assurance, image quality measurements are required. An important metric of digital imaging systems is the optical resolution, Fig. 1, which determines the image acuity [3, 24-27].

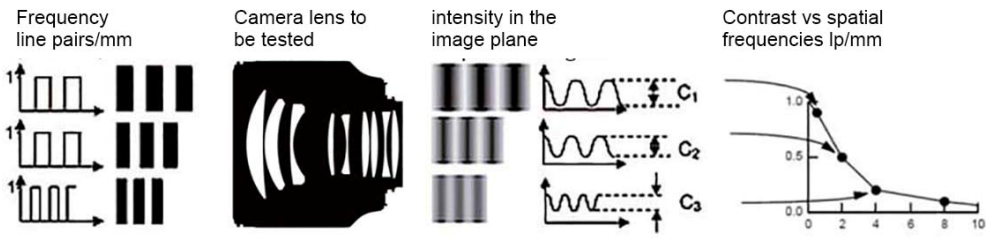

Fig. 1. Contrast transfer function vs. frequency [3-6]

Image processing algorithms are sufficiently developed and are further developing, of course, primary video is very important to have the primary information to process. The lens system in front of the optical sensor must ensure an image with less optical loss in wide range of colour shades, a wide range of contrast ratio without geometrical distortions or as low as possible. The photosensitive cells of the optical sensor must sample the

image well enough as to deliver it to the imaging processing algorithms. The resolution of the lens system is limited by the phenomenon of diffraction, which most often suffers from aberrations.

These effects lead to light scattering, low image contrast and other unwanted phenomena. Even if we had ideal lenses, without aberrations, wave properties of light make a point in the object plane to be represented in the image plane as a disk surrounded by rings of decreasing intensity, Airy disc [7].

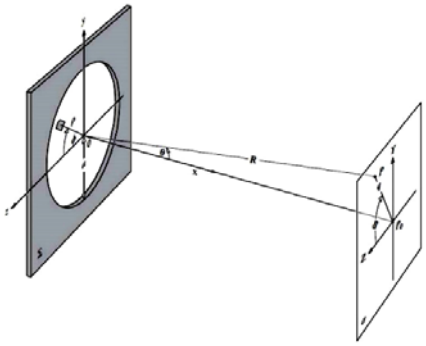

Fig. 2. Circular aperture and Fraunhofer diffraction that occur in camera lenses

The effect of diffraction becomes observable when the light waves interact with the aperture of the camera lens, when viewing point objects, the size of which is comparable to one of the dominant wavelengths of the visible spectrum.

An important optic phenomenon in the practice of designing and examining optical instruments is the Fraunhofer diffraction on a circular aperture [8].

A plane wave that interacts with the circular aperture of the camera located in plan Σ, Fig. 2, under certain interaction conditions, will create a diffraction pattern on a parallel plane at a distance x. Using lens L_2 with long focal length the observation plane σ can be brought closer to the entrance aperture Σ, Fig. 3a. The light waves which touch the entrance aperture are cut by the shape of the circular aperture (plane Σ), and in that way they are projected onto the lens L_2 to form the image in the focal plane, σ. It is obvious that the same process occurs in the human eye, in the telescope, the microscope, or camera lens. The image of a distant luminous point, given by an ideal convergent lens system, without aberrations and other optical inhomogeneities, is not a point, it is a diffraction pattern.

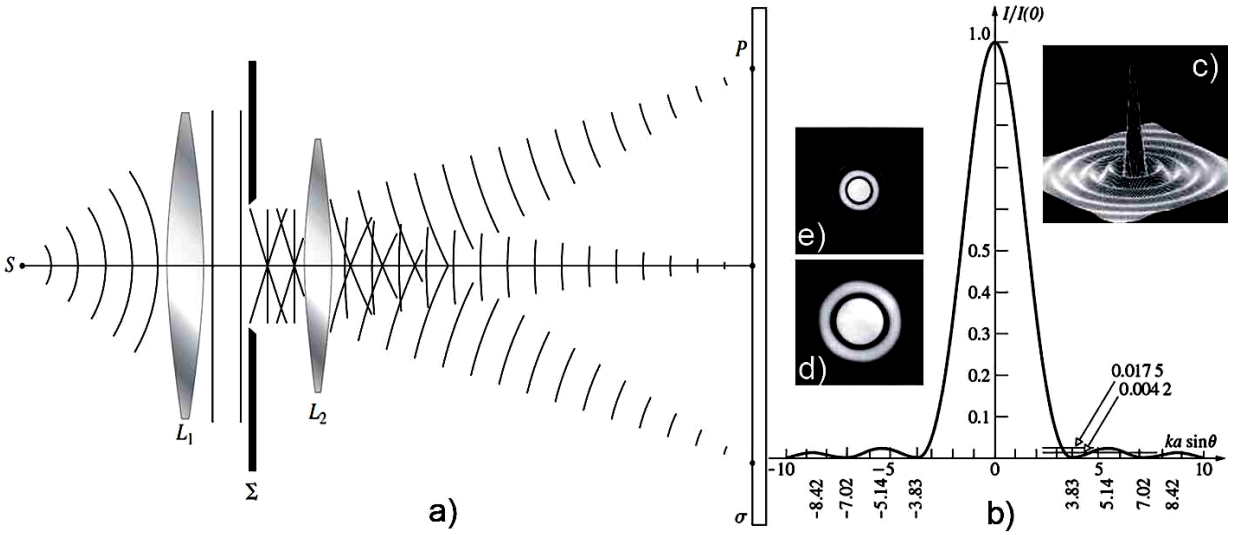

Fig. 3. (a) Optical scheme with 2 lenses for observing Fraunhofer diffraction, (b) distribution of radiation produced by diffraction on the circular aperture, (c) 3D representation, (d) Airy disc from an aperture of 0.5 mm, and (e) from an aperture of 1.0 mm in diameter

Because of the diffraction only part of the incidence wave is collected and therefore no perfect image will be formed. The phenomenon occurs sharply in the conditions in which the geometric dimensions of the examined point are comparable to the wavelength, the light waves are diffracted by the limited size circular aperture of the lens, which forms a diffraction pattern on the image plane, Fig. 3 d.

Within constant limits irradiance at point P, Fig. 2, is given by [8]:

$$I = \frac{2\varepsilon_A^2 A^2}{R^2}\left[\frac{J_1(kaq/R)}{kaq/R}\right]^2 \tag{1}$$

Irradiance in P_0 is therefore

$$I(0) = \frac{\varepsilon_A^2 A^2}{2R^2} \tag{2}$$

ε_A, signal energy per unit area, A, surface, R, distance to point P, $J_m(u)$, represents the Bessel function of the m order.

$$J_m(u) = \frac{i^{-m}}{2\pi}\int_0^{2\pi} e^{i(mv+u\cos v)}\,dv \tag{3}$$

The numerical values of which are tabulated for a wide range of u, just like sinus and cosine, $J_m(u)$, is a decreasing monotonous oscillatory function Fig. 4.

If we consider R as constant in the region of the pattern, the following equation can be written as:

$$I = I(0)\left[\frac{2J_1(kaq/R)}{kaq/R}\right]^2 \tag{4}$$

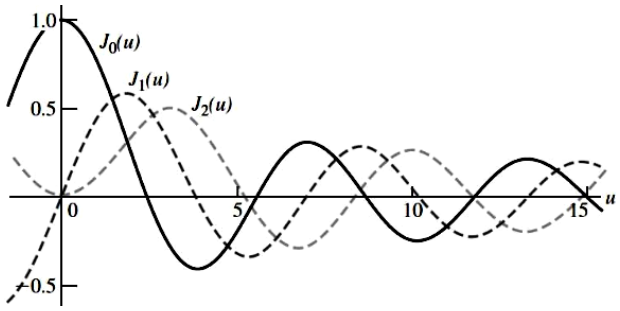

Fig. 4. Bessel functions

From Fig. 2 results $\sin\theta = q/R$, the irradiance can be written as a function of θ,

$$I(\theta) = I(0)\left[\frac{2J_1(ka\sin\theta)}{ka\sin\theta}\right]^2 \tag{5}$$

as illustrated in Fig. 3 b. Due to the axial symmetry, the central tower-like maximum corresponds to the circular spot with the highest radiation, known as Airy disc, Fig. 3 d. The central disk is surrounded by a dark ring that corresponds to the first 0 of the function $J_1(u)$. Radius q_1 from the centre to the first black disk surrounding the Airy disk, $q_1 = 3.83R\lambda/2\pi a$ (value u=3.83 resulting from $kaq/R = 3.83$ is taken from the Bessel table functions), then can be written.

$$q_1 = 1.22\frac{R\lambda}{2a} \tag{6}$$

For a lens with the focus in the plane σ, the focal distance $f \approx R$, therefore

$$q_1 = 1.22\frac{f\lambda}{D} \tag{7}$$

where D is the aperture diameter, in other words, $D=2a$, Fig. 2. The diameter of the Airy disc in the visible spectrum is approximately equal to $f/\#$ of the lens; q_1 varies inversely with diameter D. When the value of D approaches the value of λ the Airy disc rises greatly, Fig. 3 d), e), [8].

2.2. Optical spread functions

Optical transfer functions describe fundamental physical processes that manifest themselves in imaging systems. Optical imaging systems with a lens system are limited by the diffraction phenomenon, have aberrations and other optical distortions. These undesired effects scattered light in the picture. A CMOS imaging array integrates the light falling on photodetector elements, the light is effectively spread on the area defined by the dimension of the array photoelement, further spreading can occur as a result of the charge diffusion and charge transfer inefficiencies operating within the device. Point spread functions are the 'building blocks' of real images and will be responsible for the degradations in image quality (sharpness, resolution, definition, fidelity, etc.) that occur in imaging systems.

The image of a point in a linear, stationary imaging system is a function of two orthogonal variables (x, y), usually taken in the same directions as the image plane variables x_p and y_p. If the system is isotropic (i.e. it has the same physical properties in all directions), the PSF will be rotationally symmetrical, and it can thus be represented by a function of one variable, r say, where $r^2=x^2+y^2$. The function representation, $I(x, y)$, $I(r)$ - for isotropic system, units of light intensity (for optical systems); voltage, equivalent to effective exposure (CMOS).

The shape of the PSF (in particular its extent in the x and y directions) determines the sharpness and resolution aspects of the image quality produced. If the PSF is very small in the x and y directions, we can expect the image sharpness and resolution to be good.

The line spread function (LSF). The profile of the image of a line (a function of just one variable) is the line spread function (LSF). It is formed from the summation of a line of overlapping point spread functions. If the system is isotropic, the LSF is independent of the orientation, and in this case the LSF contains all the information that the PSF does. Fig. 5 shows the relation between the LSF and the PSF for a typical diffusion type imaging process.

The input to an imaging system can be thought of as a two-dimensional array of very close points of varying value (luminance). We consider a linear and stationary system, the image is formed from the addition of overlapping, scaled PSFs in the x_p and y_p directions. Due to optical loss, it is expected that the recorded image be less detailed compared to the one entering the system. We denote the input scene as $Q(x_p, y_p)$, the output image as $Q'(x_p, y_p)$ and PSF as $I(x,y)$. Mathematically, the relation between them is given by the imaging equation:

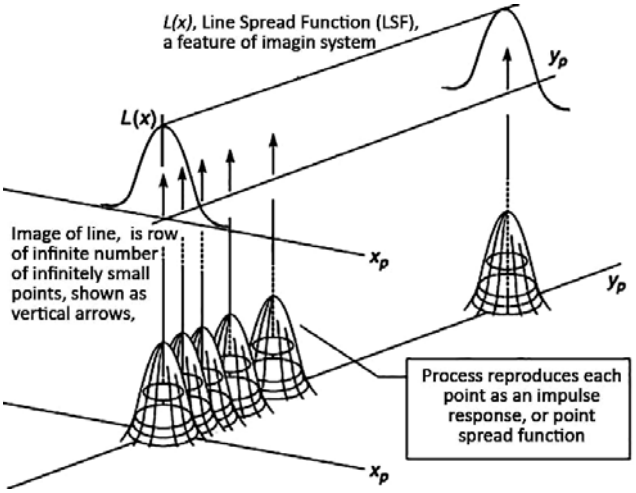

Fig. 5. Line spread function as a sum of point spread functions along a line[8]

$$Q'(x_p,y_p) = \int_{-\infty}^{\infty}\int_{-\infty}^{\infty} Q(x,y)I(x_p - x, y_p - y)dxdy \tag{8}$$

The equation is a two-dimensional convolution integral, and reflects the summation process of optical transfer of PSF scaling functions on the whole image. The integral is the summation process when the individual PSFs are infinitesimally close together. In shortened notation, $Q'(x, y)=Q(x, y) \otimes I(x, y)$ or $Q' = Q \otimes I$, where the sign $\otimes$ denotes the convolution.

Using the LSF instead of the PSF allows us to write a one-dimensional simplification:

$$Q'(x_p) = \int_{-\infty}^{\infty} Q(x)L(x_p - x)dx \tag{9}$$

where $L(x)$ is the line spread function, $Q(x)$ is the one-dimensional input and $Q'(x)$ is one dimensional output. In this case, the input scenes in the system illustrated by Fig. 5 are considered as an infinitesimally close set of lines. The image is formed from the addition of overlapping weighted line spread functions.

$$Q'(x)=Q(x) \otimes L(x) \tag{10}$$

or

$$Q' = Q \otimes L \tag{11}$$

If the inputs in a linear, stationary imaging system have a sinusoidal form, then the output also has a sinusoidal form, usually with less amplitude due to losses. The image will have the same spatial frequencies as well as the entrance ones. The degree of modulation reduction depends on the spatial frequency. The low frequencies correspond to the coarse details of the image. High frequencies have a decrease in modulation, at very high frequencies, the modulation can be completely lost, Fig. 6.

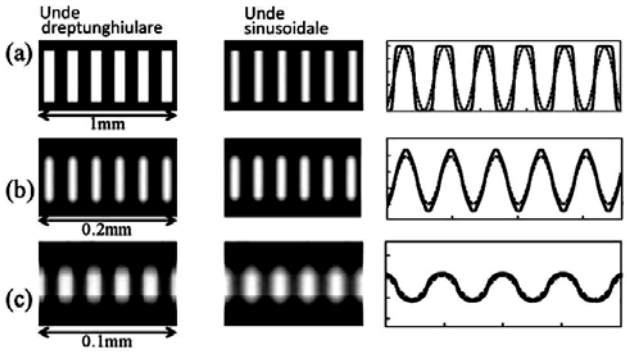

Fig. 6. Spatial frequencies and the degree of modulation reduction [9, 10]

The reduction in modulation of a particular spatial frequency ω is known as the modulation transfer factor. A graph of the modulation transfer factor against spatial frequency ω gives the modulation transfer function (MTF). Fig. 9 shows some typical curves. The MTF describes the reduction in modulation, or contrast, occurring in a particular imaging system, as a function of spatial frequency. Curve (c) illustrates an initial increase greater than 1 for low frequencies, and this is evidence of development adjacency effects and represents a non-linearity of the system [8, 9] which occurs under certain conditions.

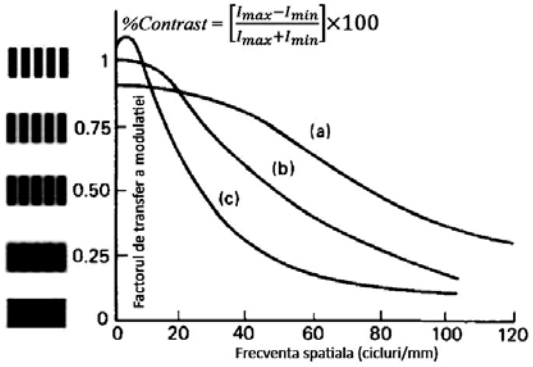

Fig. 7. MTF, modulation transfer function graph [7-10]

The Fourier analysis is successfully applied in the theory of imaging, and is an important tool for the decomposition of functions in their frequent spatial components. For a non-periodic function $f(x)$, Fourier transform $F(\omega)$ is defined as:

$$F(\omega) = \int_{-\infty}^{+\infty} f(x)\, e^{-2\pi\omega x}\, dx \tag{12}$$

where $F(\omega)$ is the number of frequencies present in the non-periodic function $f(x)$, Fig. 8. Eq. (12) can be interpreted as: for determining the amount of frequency ω, the function $f(x)$ is multiply with the sinus and cosine of this frequency. The result is the area expressed by the integral, in terms of amplitude for the given frequency [11]. The result $F(\omega)$ is called the Fourier Spectrum, or the spectrum of the function $f(x)$, of frequencies, generally continuous.

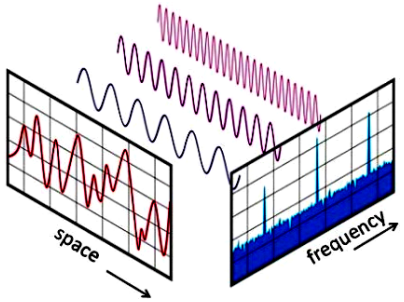

Fig. 8. Fourier decomposition [12]

The unit of measurement for ω is the number of cycles over spatial dimension x, $f(x)$ is a function of the distance (i.e., mm), therefore $F(\omega)$ is a function of the spatial frequency (mm^{-1}), which means cycles/mm (cy/mm).

The *slanted-edge method* [13], Fig. 9, illustrates the features of the ESF function building algorithm (edge spread function).

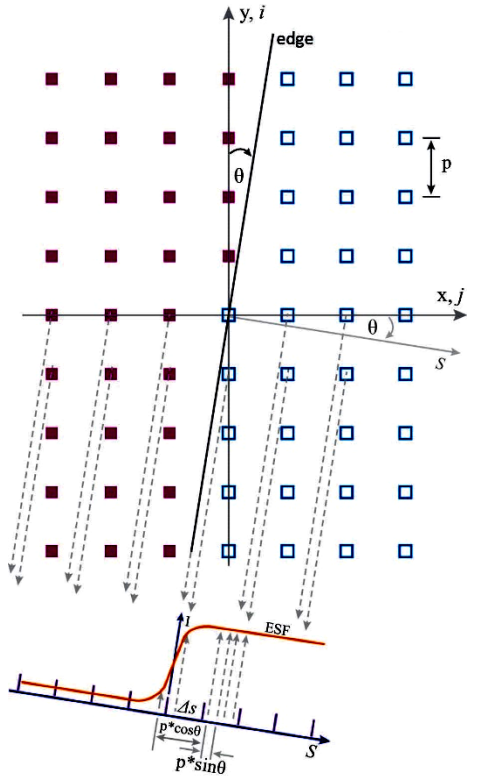

Fig. 9. Image pixels projection on coordinate axis s, perpendicular to the gradient line of light intensity, oriented at the angle θ relative to the y-direction of the pixels. The rotation of the coordinate system allows the sampling interval Δs to be smaller than the interval between pixels, thus increasing the accuracy of the recorded values [13]

The pixel lines Fig. 9 are reprojected on the coordinate axis s, inclined at the angle θ relative to the pixel orientation. The value of the ESF function depends on the distance from the gradient line. The function can be described as follows

$$E_{i_p j} = \int ESF(s)\delta(s + ip\sin\theta - jp\cos\theta)ds \qquad (13)$$

where $E_{i_p j}$ is a discrete set of samples of the function $ESF(s)$ for the pixels of row i, over a distance $s(i, j) = p(j\cos\theta - i\sin\theta)$ from the gradient line, i is the row number, j – column number, p is the pixel size that is the same in both orthogonal directions, and θ is the projection angle. The matrix $E_{i_p j}$ corresponding to different pixel rows i, depends on the variation in distance $s(i, j)$, as illustrated in Fig. 9. When N pixel rows are projected, sampling points (subpixels) accumulate on the s, forming a sampling pattern for the ESF function. Generally this sampling does not have a uniform distribution on the x-axis. The spatial distribution on the s axis depends on the pixel size p, dimension N of the pixels array, and the angle of reprojection θ. The samples E_{ij} can be reordered and collected in equal intervals Δs (*bins*) as:

$$ESF_k = \frac{1}{n_k}\sum_{i_p, j} bin(s(i,j) - k\Delta s) \qquad (14)$$

where n_k is the number of pixels whose distance from the gradient line, $s(i, j)$, falls within the interval $(k - \frac{1}{2}\Delta s)$ and, $(k + \frac{1}{2}\Delta s)$ and $bin(s(i,j) - k\Delta s)$ is the rectangular function defined to have the value of 1 for $|s(i,j) - k\Delta s| \le \frac{\Delta s}{2}$, and zero elsewhere.

Generally for a finite image array and a small reprojection angle, the variation n_k depends of the interval Δs and the pixel size, p. If $\Delta s \sim p$, a large number of reprojected pixels are averaged within each bin and the reprojection/binning operation is equivalent to a periodic sampling of the presampled ESF with a large, uniform aperture. Noise in the measured ESF is small due to the averaging of a large number of pixels, but the large aperture causes poor spatial frequency response. If $\Delta s << p$, the average number of reprojected pixels within each bin is markedly reduced; the ESF will be finely sampled, but the noise may become objectionable [13-17].

Image quality and MTF. Image quality involves psychophysiological processes of perception of the various physical characteristics of the image. The MTF characterizes those image attributes that contribute to the subjective perception of quality, such as sharpness and resolution. The term sharpness refers to the subjective impression produced by an edge of the image in the visual perception of the observer. The degree of sharpness depends on the shape and of the edge profile, the edge between different contrast regions of the image, but the perception being subjective is complex and difficult to evaluate. In the digital camera, the image clarity is determined by the lens quality, optical system, and mathematical algorithms of pixel processing. The line spread function is obtained by the numerical derivation of the edge spread function that contains the light intensity profile. Researches in recent years were oriented to establish the image quality model. In all cases, the features of the MTF curve were taken into consideration. The MTF theory is considered to be one of the most important tools available to image scientists. The Fourier theory is also

essential for the understanding of other imaging aspects such as optical information, noise and image processing.

3. The algorithm and numerical results

The camera resolution can be checked with special test charts with various spatial frequencies,

Fig. *1*, or by using the slanted-edge method. The second method involves a number of preparatory operations, a series of calculations for building the MTF function graph, contrast versus frequency, cy/px or cy/mm, or lp/mm. An advantage of the slanted-edge method is that, when we do not have a special resolution test chart or we cannot remove the camera from the device to test it on the lab bench, then we can perform slanted-edge resolution measurements, in optimum lighting conditions. Also, both methods, the resolution test chart and the slanted-edge method, complement each other.

The aim of the algorithm is to calculate the modulation transfer function. Which means: with the increase in spatial frequency, the contrast decreases (Fig. 1).

Algorithm summary:

1) a slanted-edge object is selected (Fig. 10a). Within the object frame, that contains a slant edge, is the selected region of interest, ROI, with linear edge and good contrast (Fig. 10c).

2) The image ROI is registered (Fig. 10c).

3) For each pixels line in the ROI, the centroid points are calculated (through which the slant edge passes) (Figs. 13b, 14a, 14b).

4) Using the least squares method and linear regression, the angle of the slant edge is calculated (Figs. 11, 15).

5) The edge spread function, ESF, is calculated (Fig. 16). For this, the over-sampling procedure is applied (Fig. 12b), the coordinate system is rotated at the angle calculated in p. 4), (Fig. 9, 10b, 11, 12). The coordinate axis, x', is divided into sampling intervals. ROI pixels are projected on the x' axis, which is perpendicular to the slant edge (Fig. 9, 11, 12b). The pixel average is calculated, being in each sampling interval, as a result of projection on the x axis. The ESF function is built. On the x axis, the number of sampling interval, on the y axis, pixels average value of that interval.

6) The line spread function LSF is calculated (Fig. 18), which is the result of the numerical derivation of ESF, p. 5). To eliminate the noise, the Hamming window method is applied

7) The modulation transfer function, MTF expresses quantitatively the quality of the optical system.

The method is based on a well-defined calculation algorithm. After the preparatory actions, the procedure starts by recording a slant edge at an angle of 5-7 degrees relative to the horizontal - the vertical or horizontal pixels of the CMOS optical sensor. To ensure the quality of the measurements, the edge must be as close to a straight line and it is necessary to have a sufficiently good contrast, Fig. 10 a.

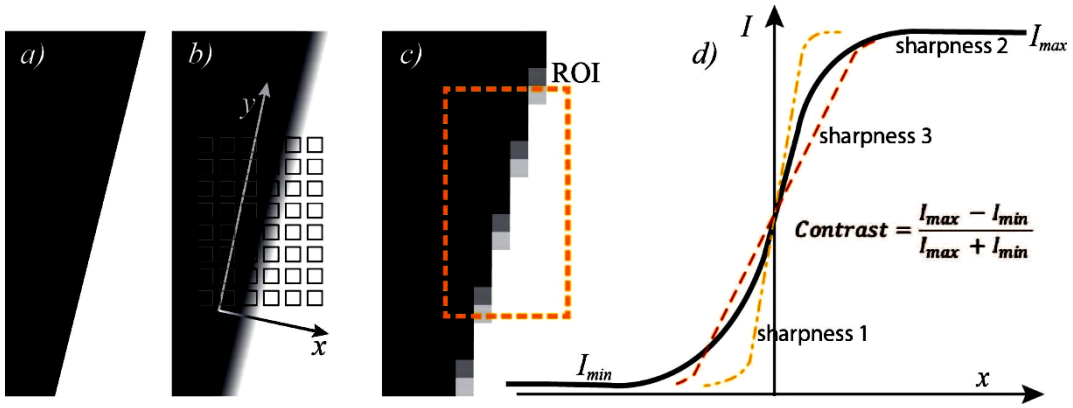

Fig. 10. (a) target object, slant edge, (b) the image of a slanted-edge object, projected onto the CMOS optical sensor pixel array, (c) example of slant edge sampling by the optical sensor array, pixel size: 0.00428 mm (4.28 μm), (d) intensity profile of slant edge, at the same contrast there may be more degrees of sharpness

The linear edge image on the CMOS sensor array appears as a light gradient from low intensity (dark area) to increased intensity, luminous area (Fig.10 b).

Therefore, the optical sensor pixels array will record the image of the slanted-edge object.

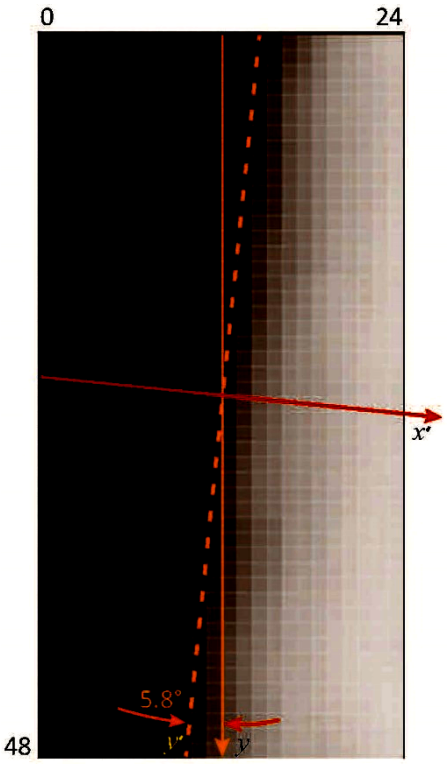

Fig. 11. Enlarged image of the registered region of interest, the oblique interrupted line is the light gradient slope, magnification x400

The slanted-edge image is always more diffused than the slanted-edge object because of the diffraction phenomenon on the lens entrance aperture, phenomenon described in the theoretical part. A statistical analysis of the pixels is performed in the nearness of the light gradient, to calculate the edge angle, which serves to build the ESF function.

The interrupted line frame, Fig. 10 c) represents the region of interest ROI, is selected so as to include a suitable part of the slant edge, from which the edge slope is calculated, the y axis, Fig. 10 b, after which the pixels are projected on the x axis, Fig. 10 b, with a sampling interval of 1/4 pixel, Fig. 12, the ESF function is built, Fig. 10 d.

The calculation method of the optical modulation transfer curve was applied to an adaptive optoelectronic system with optical sensor APS-C CMOS, 22.3x14.9 mm, diagonal of 26.8 mm 5184x3456 px, 18M, pixel size 4.28 µm/px (Canon). In this case, the optical sensor serves as a sampling device of the test image Fig. 10 b.

When performing the experimental data recorded for building the MTF curve, the recommendations of ISO 12233 have been followed.

An important feature of the method is to create the 1D profile of the intensity of the slanted light gradient of the edge, by projection of pixels located on lines parallel to the y axis, with sampled step of 1/4 pixel, Fig. 10 a and Fig. 12 b. To calculate the angle of the slant edge the centroid of each line of pixels is calculated, from top to bottom. Through the centroid points so identified, using the least square method, a line is drawn, that indicates the angle of the slant edge.

A region of interest, 48x24 pixel, has been selected from a slanted-edge image, Fig. 10 c and Fig. 11. The contrast of the selected image must be greater than 20-25%, to build the threshold function, ESF. The region of interest ROI represents a pixel array of 48 rows x 24 columns, which is analyzed line by line, to calculate the centroid for each line and calculate the light gradient slope angle, using the least square method. The pixel lines of the region of interest are illustrated in Fig. 13 a. The numbers indicate the pixel values between 0 (black) - 255 (white).

Each pixel line is derived by the convolution method of two numeric vectors, one representing the pixel line [1 x n] and another, of the FIR filter type (finite impulse response) with coefficients: [-0.5, 0.5], (response function). The calculation was made using the function: w=conv(u,v); from the MatLab library, the variable w of type array saves the result of the convolution, of the two numerical vectors u and v. Let m=length(u) and n=length(v), then w is a vector of length w=m+n-1, the k-the element of which is calculated:

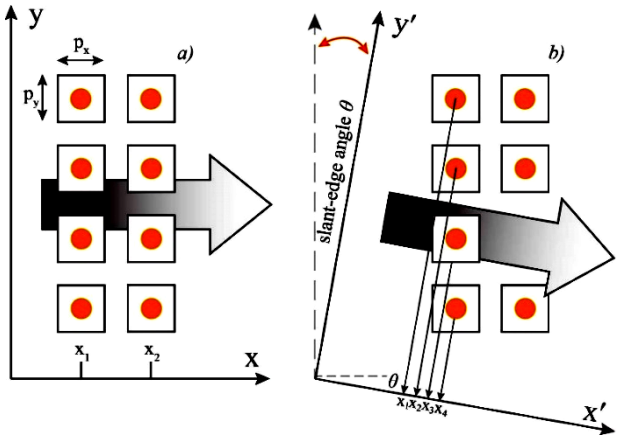

Fig. 12. Over-sampling pixels on the x-direction due to the rotation of the coordinate axis at angle θ, b).

$$w(k) = \sum_j u(j)v(k-j+1) \tag{15}$$

for all values of j, $u(j)$ and $v(k-j+1)$, for $m=n$, we obtained:

$$w(1) = u(1)*v(1)$$
$$w(2) = u(1)*v(2)+u(2)*v(1)$$
$$w(3) = u(1)*v(3)+u(2)*v(2)+u(3)*v(1)$$
$$\ldots$$
$$w(n) = u(1)*v(n)+u(2)*v(n-1)+ \ldots +u(n)*v(1)$$
$$\ldots$$
$$w(2*n-1) = u(n)*v(n)$$

The result of the convolution is exemplified by the matrix in Fig. 13 b. The centroid is the location of the pixel intensity threshold. The centroid coordinates for each line serve to the slope calculation using the least square method.

	1	2	3	4	5	6	7	8	9	10	11	12	13	14
1	38	38	39	45	52	56	64	82	106	125	151	162	177	187
2	38	38	39	46	53	59	66	83	106	124	150	161	176	186
3	40	41	38	44	51	59	69	87	110	126	152	163	178	189
4	40	41	40	44	50	59	71	90	112	127	152	163	179	189
5	40	41	42	45	49	59	75	95	115	128	153	164	179	190
6	40	41	45	45	50	60	78	100	119	131	154	165	180	191
7	40	41	46	47	51	63	82	104	124	135	155	166	181	192
8	40	41	45	48	55	66	84	106	127	141	156	167	182	193
9	40	41	44	50	58	69	84	106	130	146	157	168	183	194
10	40	41	43	50	60	71	85	106	131	149	157	169	184	195
11	39	41	41	48	58	68	82	104	130	149	164	176	191	200
12	39	41	42	48	58	69	84	106	132	150	166	177	191	201
13	39	41	42	49	59	71	87	110	135	152	170	179	192	201
14	39	41	43	49	60	73	91	115	139	154	173	181	193	201
15	39	41	45	50	61	76	96	120	143	157	176	183	192	201
16	39	41	46	51	62	78	100	125	147	160	178	183	191	199
17	39	41	46	51	62	80	103	128	149	162	179	183	190	198
18	39	41	47	52	63	81	105	130	151	163	180	183	189	197
19	36	37	47	54	67	87	110	133	152	163	181	185	192	199
20	38	38	48	55	69	89	112	135	154	165	181	185	192	200
21	39	41	50	58	72	92	115	138	156	167	181	186	192	200
22	41	44	52	60	75	95	119	141	159	169	182	186	193	201
23	42	46	54	62	78	98	122	144	161	170	183	187	193	201
24	43	48	54	63	79	100	124	145	162	171	183	187	194	202
25	42	48	54	63	80	101	125	146	162	170	183	187	194	202
26	42	48	54	63	80	102	125	146	162	170	184	188	195	202
27	44	47	56	64	78	99	121	142	158	166	186	190	197	204
28	44	48	56	64	80	100	122	143	159	167	187	191	197	205
29	46	49	57	66	82	102	124	144	160	169	188	192	198	206
30	47	51	58	69	86	107	127	146	162	172	190	194	200	207
31	49	54	60	72	92	112	131	149	165	176	192	196	202	208
32	50	56	63	77	97	117	135	153	169	180	194	197	203	209
33	51	57	66	80	102	122	139	156	173	184	195	199	204	210
34	52	58	67	83	105	125	142	158	175	186	196	199	205	211
35	50	54	68	84	107	129	146	162	176	186	196	200	206	212
36	48	53	69	85	108	130	148	164	179	189	197	200	206	212

a)

	1	2	3	4	5	6	7	8	9	10	11	12	13	14
1	-0.5	0.0	0.5	3.0	3.5	2.0	4.0	9.0	12.0	9.5	13.0	5.5	7.5	5.0
2	-0.5	0.0	0.5	3.5	3.5	3.0	3.5	8.5	11.5	9.0	13.0	5.5	7.5	5.0
3	0.5	0.5	-1.5	3.0	3.5	4.0	5.0	9.0	11.5	8.0	13.0	5.5	7.5	5.5
4	0.5	0.5	-0.5	2.0	3.0	4.5	6.0	9.5	11.0	7.5	12.5	5.5	8.0	5.0
5	0.5	0.5	0.5	1.5	2.0	5.0	8.0	10.0	10.0	6.5	12.5	5.5	7.5	5.5
6	0.5	0.5	2.0	0.0	2.5	5.0	9.0	11.0	9.5	6.0	11.5	5.5	7.5	5.5
7	0.5	0.5	2.5	0.5	2.0	6.0	9.5	11.0	10.0	5.5	10.0	5.5	7.5	5.5
8	0.5	0.5	2.0	1.5	3.5	5.5	9.0	11.0	10.5	7.0	7.5	5.5	7.5	5.5
9	0.5	0.5	1.5	3.0	4.0	5.5	7.5	11.0	12.0	8.0	5.5	5.5	7.5	5.5
10	0.5	0.5	1.0	3.5	5.0	5.5	7.0	10.5	12.5	9.0	4.0	6.0	7.5	5.5
11	0.5	1.0	0.0	3.5	5.0	5.0	7.0	11.0	13.0	9.5	7.5	6.0	7.5	4.5
12	0.5	1.0	0.5	3.0	5.0	5.5	7.5	11.0	13.0	9.0	8.0	5.5	7.0	5.0
13	0.5	1.0	0.5	3.5	5.0	6.0	8.0	11.5	12.5	8.5	9.0	4.5	6.5	4.5
14	0.5	1.0	1.0	3.0	5.5	6.5	9.0	12.0	12.0	7.5	9.5	4.0	6.0	4.0
15	0.5	1.0	2.0	2.5	5.5	7.5	10.0	12.0	11.5	7.0	9.5	3.5	4.5	4.5
16	0.5	1.0	2.5	2.5	5.5	8.0	11.0	12.5	11.0	6.5	9.0	2.5	4.0	4.0
17	0.5	1.0	2.5	2.5	5.5	9.0	11.5	12.5	10.5	6.5	8.5	2.0	3.5	4.0
18	0.5	1.0	3.0	2.5	5.5	9.0	12.0	12.5	10.5	6.0	8.5	1.5	3.0	4.0
19	0.0	0.5	5.0	3.5	6.5	10.0	11.5	11.5	9.5	5.5	9.0	2.0	3.5	3.5
20	1.0	0.0	5.0	3.5	7.0	10.0	11.5	11.5	9.5	5.5	8.0	2.0	3.5	4.0
21	0.5	1.0	4.5	4.0	7.0	10.0	11.5	11.5	9.0	5.5	7.0	2.5	3.0	4.0
22	1.5	1.5	4.0	4.0	7.5	10.0	12.0	11.0	9.0	5.0	6.5	2.0	3.5	4.0
23	2.0	2.0	4.0	4.0	8.0	10.0	12.0	11.0	8.5	4.5	6.5	2.0	3.0	4.0
24	3.0	2.5	3.0	4.5	8.0	10.5	12.0	10.5	8.5	4.5	6.0	2.0	3.5	4.0
25	3.0	3.0	3.0	4.5	8.5	10.5	12.0	10.5	8.0	4.0	6.5	2.0	3.5	4.0
26	3.0	3.0	3.0	4.5	8.5	11.0	11.5	10.5	8.0	4.0	7.0	2.0	3.5	3.5
27	1.5	1.5	4.5	4.0	7.0	10.5	11.0	10.5	8.0	4.0	10.0	2.0	3.5	3.5
28	1.5	2.0	4.0	4.0	8.0	10.0	11.0	10.5	8.0	4.0	10.0	2.0	3.0	4.0
29	2.5	1.5	4.0	4.5	8.0	10.0	11.0	10.0	8.0	4.5	9.5	2.0	3.0	4.0
30	2.5	2.0	3.5	5.5	8.5	10.5	10.0	9.5	8.0	5.0	9.0	2.0	3.0	3.5
31	3.0	2.5	3.0	6.0	10.0	10.0	9.5	9.0	8.0	5.5	8.0	2.0	3.0	3.0
32	3.5	3.0	3.5	7.0	10.0	10.0	9.0	9.0	8.0	5.5	7.0	1.5	3.0	3.0
33	3.5	3.0	4.5	7.0	11.0	10.0	8.5	8.5	8.5	5.5	5.5	2.0	2.5	3.0
34	4.0	3.0	4.5	8.0	11.0	10.0	8.5	8.0	8.5	5.5	5.0	1.5	3.0	3.0
35	3.0	2.0	7.0	8.0	11.5	11.0	8.5	8.0	7.0	5.0	5.0	2.0	3.0	3.0
36	3.0	2.5	8.0	8.0	11.5	11.0	9.0	8.0	7.5	5.0	4.0	1.5	3.0	3.0

b)

Fig. 13. (a) pixel values of ROI;(b) numerical derivation of pixel lines for calculating centroid points

An example of calculation for the 7th line of pixels Fig. 13 a is shown in the diagrams in Fig. 14. Numerical derivation helps us identify the centroid of the line, the highest bar, diagram Fig. 14 b.

After calculating the centroid for each line, the slope angle of light gradient is calculated relative to the y axis, Fig. 11, using the least squares method and linear regression. To calculate the slope, we consider the movement from one-pixel line to another as the movement on the y axis, and de centroid point distance from the beginning of the line, coordinate x.

The totality of the calculated centroid points has some distribution Fig. 15. Using the linear regression method we calculate the coefficients a and b, for the equation of the line of type f(x) = y = a + bx, which best approximates this distribution.

For a set of experimental points $x_1, x_2, \ldots x_n$; $y_1, y_2, \ldots y_n$, the value of a is determined for the slope and value of b, for intercept. The least square method consists of minimizing the sum of squares errors between the values of y_i (extracted from the experiment) and values of $f(x_i)$ calculated using the regression line. The formulas for a and b are:

$$b = slope = \frac{(n\sum x_i y_i) - (\sum x_i)(\sum y_i)}{(n\sum x_i^2) - (\sum x_i)^2} \tag{16}$$

$$a = intercept = \frac{1}{n}(\sum y_i - b\sum x_i) \tag{17}$$

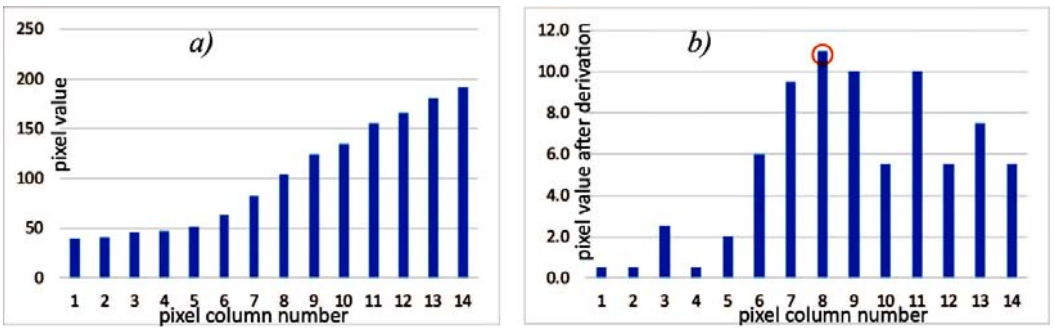

Fig. 14. (a) pixel line intensity chart, (b) numerical derivation of the pixel line for calculating the centroid, the highest bar

The summing is done from *i=1* up to *i=n*.

$$ERR - a = Slope \cdot Error = S^* \sqrt{\frac{n}{(n\sum x_i^2)-(\sum x_i)^2}} \quad (18)$$

$$ERR - b - Intercept \cdot Error = S^* \sqrt{\frac{\sum x_i^2}{(n\sum x_i^2)-(\sum x_i)^2}} \quad (19)$$

where:

$$S = \sqrt{\frac{\sum(y_i - ax_i - b)^2}{n-2}} \quad (20)$$

The parameter *a* from the equation of the regression line *y=a+bx* represents the intersection of the regression line with the *Y*, if *x=0*, then *y=a*; parameter *b* represents the slope of the line, which is the tangent of the angle between the regression line and the horizontal line, Fig. 15. If the value of *b* is positive, then the dependence between the two variables is directly proportional, the increase of the variable *x* will lead to the increase of the *y* variable, if the value of the parameter *b* is negative, then the dependence is inversely proportional, the variation in one sense or another of the variable *x* will result in a variation in the opposite direction of the *y* variable.

To note *S* is the square root of the ratio of the sum of squares of deviations from the estimated line to the number of data taken into account, more than 2, for determining the line. It can be said that the regression line represents the point of equilibrium in a bivariate distribution. The utility of the regression line is that it serves as basis for predicting *y* values associated with *x* values.

For the calculus, the MatLab function was used:

[p, s]=polyfit(n_lines, centroid_numbers, n); n_lines, is a numeric vector, which contains the number of pixel lines, *centroid_numbers*, is a numeric vector, contains the estimated centroid values, for each line, the points in variable *n_lines* correspond to those in the *centroid_numbers*, *n* represents the degree of polynomial estimation, the function returns the coefficients for the line equation that estimates the experimental data; the *p*, vector, has the length *n+1*, contains the polynomial coefficients for the least squares estimation; the *s* optional variable contains coefficients for estimating errors.

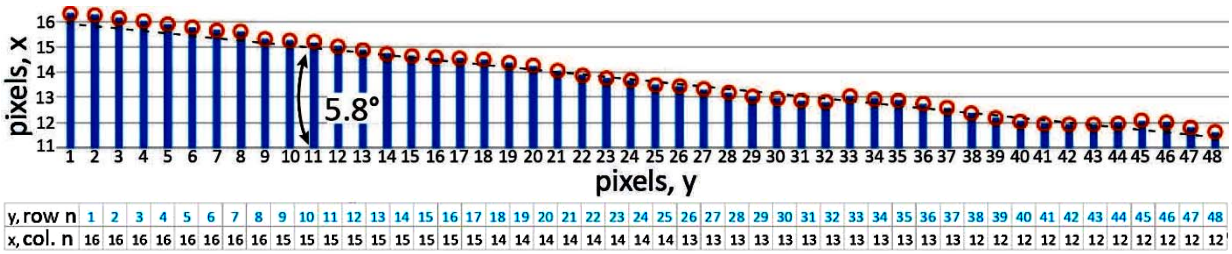

Fig. 15. Diagram of pixel lines and centroid points for each line in Fig. 13 b. For economy of space the chart is rotated at 90°; (horizontal axis, pixels(y)

The numerical vector (*centroid_numbers* [12, 16]), centroid coordinates (for each line), obtained as a result of the calculations are illustrated in Fig. 15. The slope calculated by the least square method is -0.1 or about 5.8°.

$$slope_{degrees} = \frac{180}{\pi} * arctg\big(abs(-0.1011)\big) = 5.77^{\circ} \quad (21)$$

The oblique line traced through the coordinates of the centroid represents the slope of the light gradient on the optical sensor, which helps us build the ESF function.

Axis *x′*, perpendicular to the light gradient line, Fig. 10 b, Fig. 11, Fig. 12, on which the pixels are projected, to build the ESF function, is divided into sampling intervals, the method allows an over-sampling of light gradient on the x′ direction, Fig. 12 b. In our case, the edge is relatively diffused, due to the optical phenomena on lens aperture, light diffusion on optical elements, chromatic aberrations.

After calculating the angle of the fitted margin, the ROI pixels are projected on the *x′*, oriented on the direction of propagation of light gradient, Fig. 10 b and 12. The oversampling illustrated in Fig. 9, Fig. 12 allows us to record the decrease of the intensity of the light gradient in the x direction with one pixel pitch; the projection of the pixels is calculated using the trigonometric relationship, Fig. 9, the functions in the MatLab library and the mtf calculus software sfrmat3 [12].

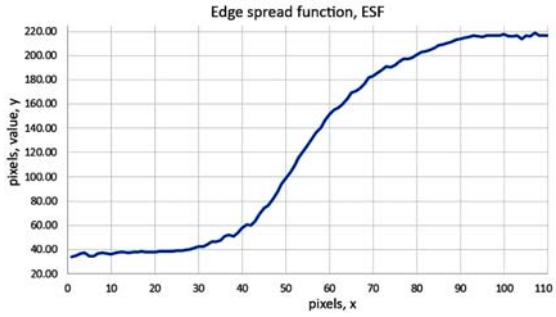

Fig. 16 Experimental graph of the ESF function, (edge spread function), the transition from the dark to the light region is a characteristic of the optical system. Lower values on the vertical axis mean darker to black, higher values, meaning lighter shades to white

The calculation of the ESF function illustrates the variation of pixels intensity in the neighbourhood of the transition from dark to bright, depending on the quality of the optical system, the threshold may be more or less abrupt. The better the quality of the system, the steeper is the threshold.

The optical system response, Fig. 10 (a), to the test object recording, slant edge of high contrast, is analogous to the response of an electronic circuit to a rectangular pulse, Fig. 17.

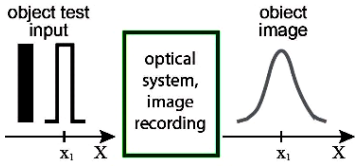

Fig. 17. Optical system response to a rectangular input pulse (black and white equally spaced bars)

The ESF function (edge spread function) contains the data needed to calculate the LSF function (line spread function), by applying the derivation operation with a function of the following form:

$$f' = \frac{f_{i+1} - f_{i-1}}{2}. \tag{22}$$

Is done as a digital filtering, by the convolution operation of the ESF function with a 1D matrix [-0.5, 0, 0.5], the result is illustrated by the LSF function graph, Fig. 18, performed with the function from the MatLab software library.

The LSF function, is the result of the numerical derivation of the ESF function, Fig. 16 represents the light gradient intensity distribution from black to white, on the propagation direction, the x′ axis Fig. 11. It has the shape of a Gaussian pulse. This type of pulse can be decomposed into Fourier series of frequencies, by applying the DFT (Discrete Fourier Transform) and FFT (Fast Fourier Transform) analysis.

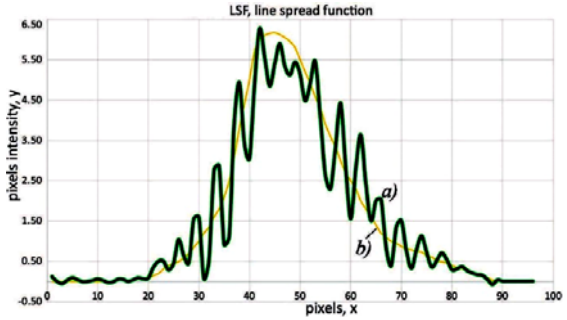

Fig. 18. Line spread function, a) obtained by deriving the ESF function, Fig. 16 for noise elimination, the numerical filtering procedure was applied, b) the signal after applying the numerical filtering procedure, the Hamming window, and other smoothing methods

Convolution. The elements of the numerical vector x [n] contain average values of the intensity in the vicinity of the slant edge, x[n] can have several hundreds of elements with values between 0-255 (depending on the ROI size). The result of the 1D convolution of two discrete signals is the rate of increase or decrease of the values in the space defined by the vector x[n], or the 1st derivative of the ESF function, Fig. 16 illustrates the method of convolution of two signals, x[n]=[34.200, 35.125, 37.000, 37.556, 34.714 ...] and h[n]=[0.500, 0, -0.500]. The vector h[n] (response function) is mirrored, then overlaps with the first term of x[n] and slides to the end of the value string of x[n]. The numbers that are one beneath another are multiplied then summed, according to the formula

$y[k] = \sum_{n=0}^{N} x[n] * h[k-n]$

k=m+n-1=5+3-1=7; n=5

1) y[0]=x[0]*h[0] = x[0]*h[0]=34.200*0.5=17.100
2) y[1]=x[0]*h[1]+x[1]*h[0]=34.200*0+35.125*0.5=17.5625
3) y[2]=x[0]*h[2]+x[1]*h[1]+x[2]*h[0]=
   34.200*-0.5+35.125*0+37.000*0.5=1.4
4) y[3]=x[1]*h[2]+x[2]*h[1]+x[3]*h[0]=
   31.125*-0.5+37.0*0+37.556*0.5=1.2153
5) y[4]=x[2]*h[2]+x[3]*h[1]+x[4]*h[0]=
   37.0*-0.5+37.556*0+34.714*0.5=-1.1429
6) y[5]=x[3]*h[2]+x[4]*h[1] =37.556*-0.5+34.714*0=-18.778
7) y[6]=x[4]*h[2]=37.714*-0.5=-17.357

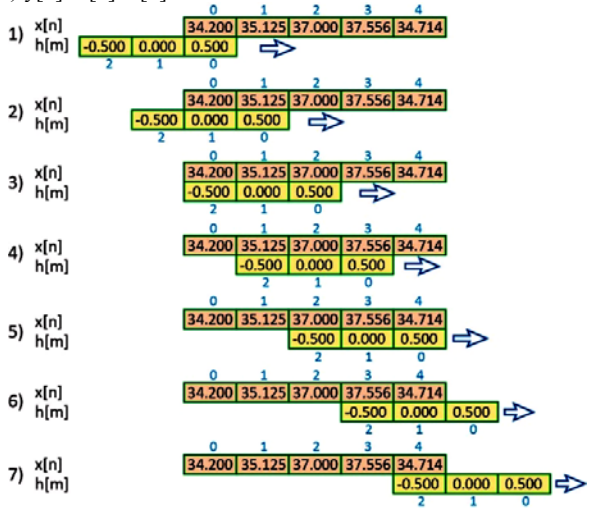

Fig. 19. Convolution of two signals, represented by two unidimensional matrices

The modulation transfer function, Fig. 20, is calculated by the Discrete Fourier Analysis of the Line spread function, Fig. 18. Before applying DFT, the LSF function will multiply with a Hamming window type function, to prevent discontinuity errors.

The MTF analyses the imaging optical system quantitatively. Quantify the resolution power for each spatial frequency, 10, 20, ... n, line pairs/mm. As the frequency of line pair increases, the contrast between the white and black lines decreases, and is given by system limitations, optical aberrations, diffraction on the lens aperture, light diffusion, etc. The contrast is defined as:

$$C = \frac{I_{max}-I_{min}}{I_{max}+I_{min}}. \quad (23)$$

Optical contrast input, $C_{in} = \frac{(100-0)}{100+0} = 1.0$ for all spatial frequencies, Contrast system output,

$$C_{out(\frac{0.05cy}{px})} = \frac{83-17}{83+17} = 0.67; \; C_{out(\frac{0.1cy}{px})} = \frac{63-37}{63+37} = 0.26$$

$$C_{out(\frac{0.15cy}{px})} = \frac{55-45}{55+45} = 0.10$$

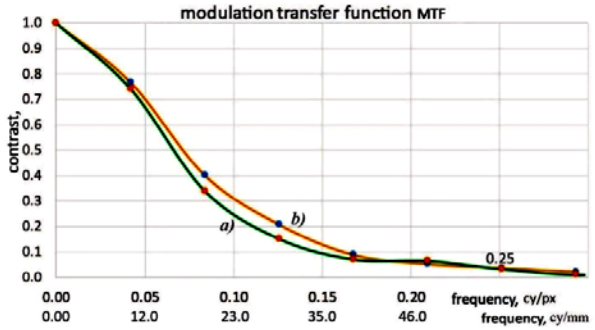

Fig. 20. The MTF function, calculated by the Fourier series decomposition of the LSF function. On the horizontal axis the values are in cy / px or cy / mm. Cycle is a signal period. A white bar and a black bar of equal width, is a cycle. For representation in cy/mm, the value cy/px, will be divided into pixel size in mm, for example for a pixel size of 4.28 μm and frequency 0.1 cy/px, we will divide 0.1: 0.00428 = 23 cy/mm or 23 line pairs/mm. Curve a) - original signal without noise filtering, b) noise reduction via signal processing

The MTF curve can take various shapes, steeper or wider, depending on the particular optical system, different slopes on certain spectral segments. This is a measure that reflects the performance of the imaging system.

The calculus was performed using the MatLab function, *y=fft(x,n)*, *x*, is the numerical input vector, data describing the LSF function, numerical vector of n elements. For discreet numerical data, the base for spectral analysis is the known method Discrete Fourier Transform. DFT transforms data describing space distribution into data describing the frequency space.

DFT for vector *x*, of length *n*, is another *y* vector of length *n*:

$$y_{p+1} = \sum_{j=0}^{n-1} \omega^{jp} x_{j+1} \quad (24)$$

ω is the complex frequency, $\omega = e^{\frac{-2\pi}{n}}$

The notation uses *i* for the imaginary unit, *p* and *j* for indexing from *0* to *n-1*.

The vector data *x* is separated by a constant interval in space or time, $dt=1f_s$ or $ds=1/f_s$, where *f* is the sampling frequency. The Fourier transform *y* has complex values. Absolute value of y_{p+1} measures the amount of frequency $f=p(f_s/n)$ present in the data.

When light is transmitted through the lenses, there is loss of intensity, light diffusion, optical distortions, optical aberrations, circular aperture diffraction, all these losses lead to decreased resolution and contrast in imaging optics. The MTF curve is a useful characteristic to quantify these losses.

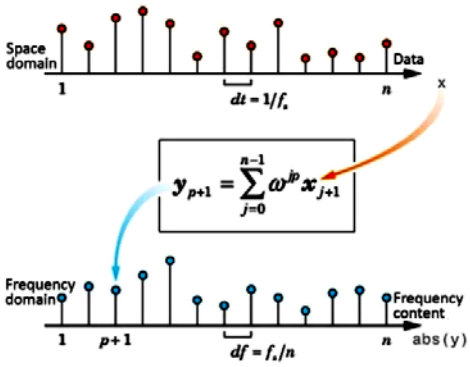

Fig. 21. Fourier transform

The calculations were performed using the Microsoft Excel, Matlab, and sfrmat3 programs. We would like to express our gratitude to the creators of these extraordinary computing tools.

4. Conclusions

The obtained results are a contribution to the application and testing of the slanted-edge method to test the resolution of new optoelectronic devices. The role of monitoring systems for security objectives with varying degrees of risk is still important and topical. The novelty of the research resides in the application of the slanted-edge method to study a featured photoelectronic device with adaptive optics, used in control and security applications. During the operation of the device, the optical parameters may deviate from the functional values due to mechanical vibrations, for example or other factors, degradation of front-facing protective coatings, other factors that can influence the resolution. The slanted-edge method focuses on soft procedures, allowing for remote resolution estimation, and it is sufficient to found an acceptable, sufficient enough, quality margin for registration

Optical resolution testing using the slanted-edge method is topical and useful in that it does not need a specialized control stand equipped with expensive test charts.

The current CMOS and CCD optical sensors are powerful enough to be used to test the lenses of the optical system. If in the past, to test the camera lens, a micrometric linear aperture and a microdensitometer to record the LSF function profile were used, today, the camera's own sensor provides us with sampling frequencies of the order of pixel size, for example 1.2 ÷ 4.28 μm, resulting in a maximum sampling frequency of 0.5 cy / px (Nyquist) = 0.5cy / 0.0012mm = 416 cy / mm, sufficient to test an optical system.

The method has also certain limits. For example, the attempt to test the chromatic resolution of the optoelectronic device with a slant edge of orange colour resulted in unsatisfactory results. The orange colour in optoelectronic devices is obtained from Red and Green in various properties (e.g. R = 247, G = 179, B = 0). The Bayer filter of the CMOS sensor interprets and generates colours according to its predefined algorithms, the lenses can have unequal chromatic resolution. A low contrast image is generated at the output. Researches will continue. Many colour shades are corrected by the sensor, but this leaves us away from real optics measurements.

During the testing, it is necessary to disconnect the contrast and sharpness functions to avoid inducing the calculation errors by artificially altering the pixel intensity.

The image of the slanted-edge object before building the ESF must be carefully analysed to select the ROI (region of interest) suitable for calculations. The ROI region and the ESF function are the starting point of the calculations

As the image of the slant edge is more diffused, the optical system has more imperfections.

MTF of a colour image does not differ significantly from the MTF of the gray scale image. Therefore, in some cases, the image ROI can be simplified, converted to gray scale to reduce the amount of computation.

The slanted-edge testing method of an optic lens system composed of lens adapters, filters, and optical sensors offers acceptable system resolution results. However, the apparent simplicity of the method requires a lot of accuracy, an initiation into the particularities of the measurement system. The slant edge must be smooth enough to minimize image defects.

The described method is universally applicable, for thermal imaging cameras, infrared imaging cameras, X-rays imager, medical imaging and radiological anatomy. It is a complement to the methods that use special test charts of advanced micrometric precision, linear micrometric slits. The method does not replace the classic method with precision test chart that is necessary for sagittal and tangential testing.

To increase the accuracy and minimize the errors, the edge angle should be 7°-10° from the vertical or horizontal pixel line.

The accurate performing of the recommended steps of the ISO 12233 and the thorough documentation ensure the satisfactory reproducibility of the measurement results.

Acknowledgements

We express our thanks to our colleagues, of Optoelectronica 2001SA, for the materials and equipment provided and for the useful observations on the methods of calculating and processing the digital signals.

References

[1] B. Tatian, J. Opt. Soc. Amer. **55**, 1014 (1965).
[2] F. H. Perrin, J. S. M. P. T. E., (69) 1969.
[3] Opticos Corporation, How to measure MTF and other properties of lenses, 1999.
[4] www.trioptics.com, available https://www.trioptics.com/knowledge-base/mtf-testing-measurement-inspection-modulation-transfer-function/.
[5] stanfordcomputeroptics.com, available: http://stanfordcomputeroptics.com/download/resolution_iccd_mtf.pdf.'
[6] www.photoblog.com, available: https://www.photoblog.com/learn/prime-vs-zoom-lenses-which-is-best/.
[7] Ralph E. Jacobson, The Manual of Photography, ninth edition,, Focal Press, Oxford, Auckland Boston, 2000.
[8] Eugene Hecht, Optics, 5ed,, Adelphi University, Boston, Columbus, Indianapolis, New York, San Francisco, Pearson Education Limited, Edinburg Gate, Harlow Essex CM20 2JE England, 2017.
[9] Shuma Horiuchi, Shuhei Yoshida, Manabu Yamamoto, Optics Express **21**(6), 7373 (2013).
[10] Available: https://blocknotfotografa.ru/mtf-modulation-transfer-function-chastotno-kontrastnye-xarakt/.
[11] Marinica Mirzu, Teodor Necsoiu,, Metode moderne ale opticii pentru calculul sistemelor optoelectronice, Bucuresti: Institutul de Optoelectronica-S.A. (IOEL-S.A.), 1998.
[12] FFT-Time-Frequency-View, Available: https://commons.wikimedia.org/w/index.php?curid=64473578.
[13] P. Burns, Slanted-edge Analysis for digital camera and scanner, International Imaging Industry Association, 12 May 2015.
[14] D. Savastru, S. Miclos, N. Iftimia, M. A. Calin, R. Savastru, D. Manea, S. Dontu, J. Optoelectron. Adv. M. **18**(11-12), 993 (2016).
[15] I. Dancus, S. T. Popescu, A. Petris, Optics express **21**(25), 31303 (2013).
[16] C. Spulber et al., 13th International School on Quantum Electronics, Bourgas, Bulgaria Sep20-24,2004; Book Series: Proceedings of TheSociety of Photo-Optical Instrumentation Engineers (SPIE); **5830**, 434 (2005).
[17] D. Craciunescu, P. Sterian, L. Fara, A. Bobei, A. Diaconu, F. Dragan, Optoelectron. Adv. M. **11**(5-6), 298 (2017).
[18] A. Hornberg, Handbook of Machine Vision, Weinheim: WILEY-VCH Verlag GmbH & Co KgaA, 2006.
[19] Constantin Rosu et al., Modern Physics Letters B **24(**1), 65 (2010).
[20] A. A. Popescu, R. Savastru, D. Savastru et al., Digest Journal of Nanomaterials and Biostructures **6**(3), 1245 (2011).
[21] C. Roşu, D. Manaila-Maximean, V. Cîrcu, Y. Molard, T. Roisnel, Liquid Crystals **38**(6), 757 (2011).

[22] A. R. Sterian, in International Conference on Computational Science and Its Applications 2007 Aug 26, p. 436, Springer, Berlin, Heidelberg.
[23] D. A. Iordache, P. Sterian, A. R. Sterian, F. Pop, International Journal of Computers Communications & Control. **5**(5), 744 (2010).
[24] S. Miclos, D. Savastru, R. Savastru, I. Lancranjan, Composite Structures **183**, 521 (2018).
[25] T. Necsoiu, G. Bostan, P. Sterian, J. Optoelectron. Adv. M. **19**(11-12), 729 (2017).
[26] M. Sohaciu, S. Ciuca, D. Savastru, G. Coman, A. Predescu, A. Berbecaru, C. Cotrut, E. Matei, I. A. Gherghescu, C. Predescu, Optoelectron. Adv. M. **10**(3-4), 257 (2016).
[27] C. Rosu, D. Manaila-Maximean, A. J. Paraskos, Modern Physics Letters B **16**(13), 473 (2002).

*Corresponding author: georgebostan@gmail.com